Chapter

The State-of-the-Art of Brillouin Distributed Fiber Sensing

Cheng Feng, Jaffar Emad Kadum and Thomas Schneider

Abstract

The distributed Brillouin sensing technique has been developed rapidly since its first demonstration three decades ago. Numerous investigations on the performance enhancement of Brillouin sensors in respect to spatial resolution, sensing range, and measurement time have paved the way to its industrial and commercial applications. This chapter provides an overview of different Brillouin sensing techniques and mainly focuses on the most widely used one, the Brillouin optical time domain analysis (BOTDA). The history and the development of Brillouin sensing regarding the performance enhancement in various methods and their records will be reviewed, commented, and compared with each other. As well, related sensing errors and limitations will be discussed, together with the corresponding strategies to avoid them.

Keywords: stimulated Brillouin scattering, distributed fiber sensing, nonlocal effects, modulation instability, pump depletion, polarization fading, spatial resolution, dynamic sensing

1. Introduction

Since optical fibers can be used to measure a variety of physical parameters directly or indirectly, sensing in optical fibers has been intensively investigated in the past few decades [1]. Fiber optic sensors can be split into two big categories, that is, point and distributed sensors. The former type, such as the fiber Bragg grating (FBG), measures the physical parameters only at a particular location but with relative high resolution and sensitivity. The detectable range of the latter one, such as optical time-domain reflectometry (OTDR) [2], is relatively large (usually the fiber length itself) and continuous but with only moderate resolution and limited sensitivity [3]. However, numerous investigations have been carried out to design a novel sensor with the advantages of both types, but avoiding their disadvantages.

With a moderate spatial resolution in the range of 1 m, distributed Brillouin sensing offers a more cost-effective solution than applying numerous point sensors in long-range sensing and a more accurate result than traditional distributed sensing methods such as OTDR [4]. Due to the recent success in breaking the limits of numerous sensing parameters such as spatial resolution, sensing range, and measurement time, the Brillouin sensing technique has proved its eligibility in a variety of fields. Thus, it has aroused significant interest in many different applications like civil engineering, oil and gas pipelines leakage monitoring, and other infrastructure surveillance tasks.

2. Basics of SBS

2.1 Spontaneous and stimulated Brillouin scattering

Brillouin scattering, named after the French physicist Léon Brillouin, who theoretically predicted light scattering by a thermally excited acoustic wave (phonon) in 1922 [5], is one of the most prominent nonlinear effects in optical fibers [6]. For spontaneous Brillouin scattering (SpBS), an incident photon (pump wave) is transformed into a frequency-downshifted scattered photon (Stokes wave) and a phonon (acoustic wave). The angular distribution of the Stokes wave is governed by the laws of momentum and energy conservation, that is,

$$\vec{k_A} = \vec{k_p} - \vec{k_s} \qquad \omega_B = \omega_p - \omega_s \tag{1}$$

where $\vec{k_A}$, $\vec{k_p}$, and $\vec{k_s}$ are the wave vector of acoustic, pump, and Stokes wave, and ω_B, ω_p, and ω_s are their corresponding angular frequencies. Considering the fiber geometry and provided that the phonon frequency is much smaller than that of both photons, an efficient Brillouin scattering only occurs in the backward direction. The Brillouin frequency shift (BFS) $\nu_B = \omega_B/2\pi$ is estimated to be ~11 GHz for typical single mode fibers (SMF) and a pump wavelength in the C-Band of optical telecommunications (around 1550 nm) [7]. As has been shown very recently, forward SBS [8] can be used for sensing applications as well [9, 10]. However, the interaction is governed by transverse acoustic modes, and compared to backward SBS, the effect is rather weak. Since a description of this new field of SBS in sensing would go far beyond the scope of this book chapter, hereafter only backward SBS and its applications are discussed.

The basic origin of SBS is electrostriction, which tends to compress the material in the presence of an electrical field [11]. The superposition of the pump and the counterpropagating Stokes wave modulates the density and hence the refractive index of the optical fiber through electrostriction. Thus, a moving grating (an acoustic wave) is formed. If the velocity of this moving grating coincides with the speed of sound in the material, the effect is very efficient and it additionally reflects optical power from the pump wave. Due to the Doppler effect, the reflected pump wave is downshifted in frequency by the frequency difference between pump and probe and thus adds power to the Stokes wave. Therefore, a positive feedback loop is established. This transformation from SpBS to SBS can be quantitatively described by the differential equation system (DES) in the propagation direction z as:

$$\begin{aligned} \frac{dI_p}{dz} &= -g_B(\omega) I_p I_s - \alpha I_p \\ -\frac{dI_s}{dz} &= g_B(\omega) I_p I_s - \alpha I_s \end{aligned} \tag{2}$$

where I_p and I_s are the intensity of pump and Stokes wave, α is the fiber attenuation, and $g_B(\omega)$ is the SBS gain.

The threshold of SBS is defined by the critical power that characterizes the transformation from SpBS to SBS. However, its definition is rather controversial. Smith et al. first defined it as the input pump power at which the backscattered power equals to the transmitted power at the output [12] and Eq. (3) with the critical gain factor $C_{th} \approx 21$ gives an estimation of this critical value:

$$P_{th} \equiv C_{th} \frac{A_{eff}}{g_B(\omega_B) L_{eff}} \tag{3}$$

where $g_B(\omega_B)$ is the peak SBS gain, $L_{eff} = [1 - \exp(-\alpha L)]/\alpha$ is the effective length with L as the real fiber length, A_{eff} is the effective cross section of the fiber, and P_{th} is the estimated SBS threshold. Later on, this estimation has been revised with different theories and approximations, achieving also different C_{th} values [13–15]. However, instead of a constant, C_{th} has been recently found to be dependent on the fiber length and its parameters [16]. As a typical experimental example, **Figure 1(a)** illustrates the transmitted and the reflected power as a function of the incident power in a 20 km SMF. The dashed black line symbolizes the SBS threshold, beyond which the backscattered power rapidly increases and the output pump power stays almost constant.

2.2 The Brillouin gain

The transferred energy from the pump to the Stokes wave can be regarded as an amplification when it is frequency downshifted to the pump wave by BFS. For typical SMF in the C-Band of optical telecommunications, the lifetime T_B of the phonon involved in the SBS interaction is usually in the magnitude of ~10 ns, which leads to a finite spectral distribution of the SBS gain. The complex SBS gain coefficient, which depicts the evolution of the probe wave as a function of frequency detuning ω between pump and probe wave, is approximated by a Lorentzian shape [17]:

$$g(\omega) = \frac{g_0 P_p}{1 - 2j(\omega - \omega_B)/\Gamma_B} \tag{4}$$

where $\Gamma_B = T_B^{-1}$, P_p is the pump power, g_0 is related to the inherent material Brillouin gain g_p with $g_0 = g_p/A_{eff}$ and A_{eff} is the effective cross section of the fiber, g_p is in the range of 3×10^{-11} m/W to approximately 5×10^{-11} m/W at 1550 nm. The real part of Eq. (4) represents the power amplification of the probe wave, also known as the Brillouin gain spectrum (BGS), and can be expressed as:

$$g_B(\omega) = \frac{g_0 P_p (\Gamma_B/2)^2}{(\omega - \omega_B)^2 + (\Gamma_B/2)^2} \tag{5}$$

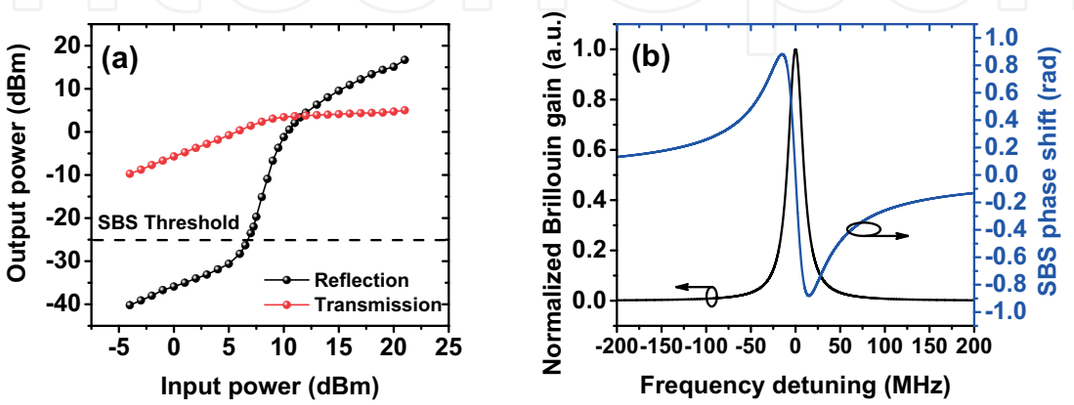

Figure 1.
(a) The transition from SpBS to SBS in a 20 km SMF, from a distinct threshold (here C_{th}≈16), the reflected stokes power drastically increases, whereas the transmitted pump power stays almost constant; (b) simulated normalized Brillouin gain spectrum (BGS) and Brillouin phase spectrum (BPS) of a 20 km SMF.

The full width at half maximum (FWHM) of the BGS $\Delta\nu_B = \Gamma_B/(2\pi)$, also known as the natural Brillouin linewidth, is estimated to be several tens of MHz for SMF, as shown in **Figure 1(b)** for a 20 km SMF. The Brillouin linewidth can be engineered to several GHz with a broadened pump for applications such as SBS-based filters [18–20] and slow light [21–23] while it can also be narrowed to a record of 3.4 MHz with specific techniques [24–28].

It is also worth to mention that the complex SBS gain changes not only the probe wave in amplitude, but also in phase by its imaginary part. As shown in **Figure 1(b)**, the SBS phase shift has a linear dependence on the frequency detuning in the vicinity of the BFS and zero-phase shift directly at the BFS, that is, the peak Brillouin gain. These properties are important for applications such as SBS-based microwave photonic filters [29] and distributed Brillouin dynamic sensing [30].

2.3 The polarization effect of SBS

Since the state of polarization (SOP) of the probe and pump waves hover randomly in the fiber due to the weak birefringence of SMF and only an averaged interaction can be detected at the output, the dependence of the SBS gain on the SOP has been neglected for long. However, with the rise of the polarization maintaining technique [31], the polarization effect of SBS has been investigated, and it has been found that the SBS efficiency of the pump-probe interaction with arbitrary polarization states is governed by [7]:

$$\eta_{SBS} = \frac{1}{2}(1 + \hat{s} \cdot \hat{p}) = \frac{1}{2}\left(1 + s_1 p_1 + s_2 p_2 - s_3 p_3\right) \tag{6}$$

where $\hat{s} = (s_1, s_2, s_3)$ and $\hat{p} = \left(p_1, p_2, p_3\right)$ represent the unit vectors of Stokes and pump waves in the Poincaré sphere. As shown in Eq. (6), the SBS efficiencies of a parallel and orthogonal SOP are $1 - s_3^2$ and s_3^2. The SBS efficiency reaches zero when both of the pump and Stokes are orthogonally linear polarized ($s_3 = 0$). This behavior can be used for many different applications from filters [19, 32, 33] via high-resolution spectrum analyzers [34–36] to the generation of THz waves [37, 38].

3. Principle of distributed Brillouin sensing

According to the DES of SBS, the Brillouin gain in each fiber section is accumulated in an SBS interaction between two continuous waves (CW). This accumulation along the fiber leads to a relative high energy conversion at the detector but makes it difficult to distinguish the information of local interactions. Therefore, distributed Brillouin sensing uses other techniques.

3.1 Temperature and strain-dependent Brillouin frequency shift

According to the theory of material science, the velocity of the longitudinal acoustic mode in the fiber depends on material properties such as Young's moduli and the density [39]. This high sensitivity to the temperature and tensile strain makes the BFS also temperature [40] and strain [41] dependent. The linear dependence has been proved and measured in several papers [40–42], as illustrated in **Figure 2** and can be expressed as:

$$\nu_B(T, \varepsilon) - \nu_B(T_0, \varepsilon_0) = C_\varepsilon \cdot \delta\varepsilon + C_T \cdot \delta T \tag{7}$$

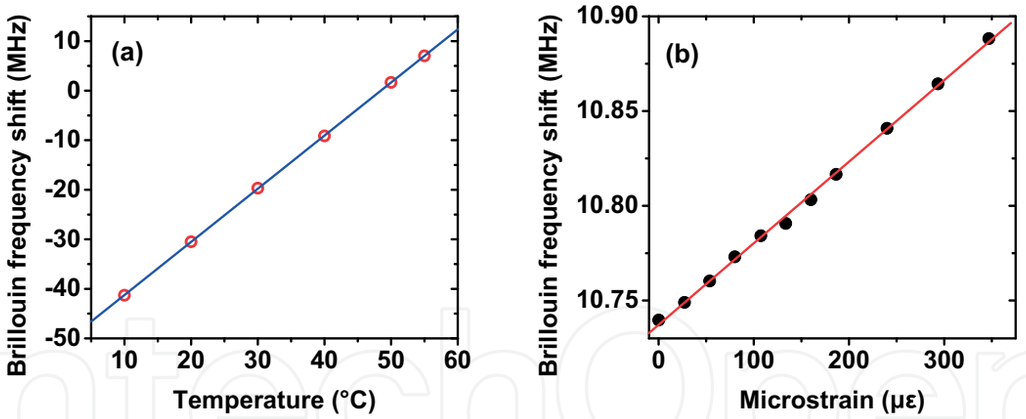

Figure 2.
BFS dependence on (a) temperature and (b) strain in a SMF for a pump wavelength of 1550 nm [42].

where $\nu_B(T, \varepsilon)$ represents the BFS at a temperature T and strain ε, C_T and C_ε are the temperature and strain coefficients. Although both temperature and strain contribute to the BFS shift, the physical difficulty in discriminating the response from these two factors can be solved with specific strategies [43]. For standard SMF, C_T and C_ε are measured to be 1.081 MHz/°C and 42.93 kHz/με, respectively [42]. The slope of the linearity has also been studied intensively and optimized with different doping concentrations [44].

3.2 Overview of SBS sensing techniques

Since the first demonstration of the most widely used distributed Brillouin sensing scheme in time domain [4], which is now called Brillouin optical time domain analyzer (BOTDA), several different schemes have been proposed and developed with their own advantages and disadvantages.

3.2.1 BOTDA

The principle of BOTDA is based on the Brillouin interaction between a pulsed pump (or probe) wave and a counterpropagating CW probe (or pump) wave. The acoustic wave is generated locally at the point where the pump pulse and the probe CW meet. The energy transfer via the acoustic wave at each position of the fiber under test (FUT) is determined by the frequency detuning between the two signals in comparison to the phonon frequency, that is, the probe wave is amplified when $\nu_p - \nu_s = \nu_a$ and depleted when $\nu_s - \nu_p = \nu_a$ where ν_p, ν_s, and ν_a are the pump, probe, and phonon frequency, respectively. As shown in **Figure 3(a)** as a typical example, local Brillouin gain (or loss) can be translated from the time-dependent to the distance-dependent information according to the round trip relation $z = ct/(2n)$ where z is the fiber position where pump and probe wave interact, t is the propagation time of the pulse, c is the velocity of light in vacuum, and n is the refractive index.

In order to derive the local BFS at each position of the fiber, the reconstruction of the BGS, as illustrated in **Figure 3(b)**, should be carried out by a frequency sweep with every frequency detuning around the phonon frequency. The accurate BFS at each fiber section can be achieved by fitting every measured BGS with the theoretical profile (either Voigt [45] or Lorentzian, dependent on pulse width) as illustrated in **Figure 4(a)**.

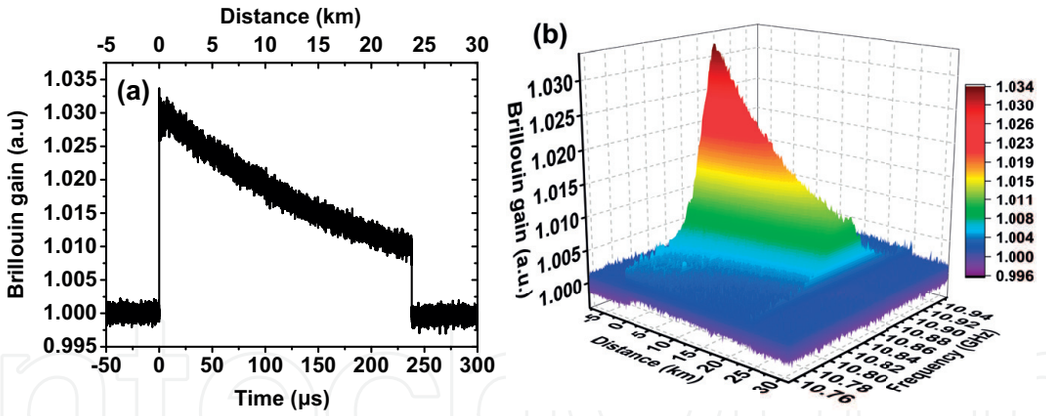

Figure 3.
(a) Evolution of the Brillouin gain for a given frequency detuning; (b) reconstructed 3D BGS along the fiber.

3.2.2 BOTDR

The principle of Brillouin optical time domain reflectometry (BOTDR) is a Brillouin scattering-based OTDR [2]. Different from BOTDA, only a pulsed pump is launched into the FUT from one side of the fiber. Since the time-resolved probe signal is back reflected due to SpBS instead of SBS, the signal power is much weaker than for BOTDA [4] and it is of great importance to apply a coherent detection with a strong local oscillator simultaneously [46]. Since an access to the other fiber end is not necessary, BOTDR is advantageous for some applications. However, besides the weak received signal, it suffers from further disadvantages such as limited spatial resolution of around 1 m, the distortion from Rayleigh backscattering, Fresnel reflection from the connector, and a limited sensing range due to fiber attenuation.

3.2.3 BOCDA

The Brillouin optical correlation domain analyzer (BOCDA) is one of the most recently demonstrated Brillouin sensing techniques. Compared to BOTDA and BOTDR, much higher spatial resolutions down to several millimeters can be achieved [47]. Its principle is based on the interaction of two identically frequency-modulated (FM) counterpropagating CW waves. Similar to the principle of a standing wave (see **Figure 5**), the frequency difference between the counterpropagating pump and probe wave remains constant at specific positions of the fiber, that is, correlation peaks called nodes. Brillouin interactions will take place at these

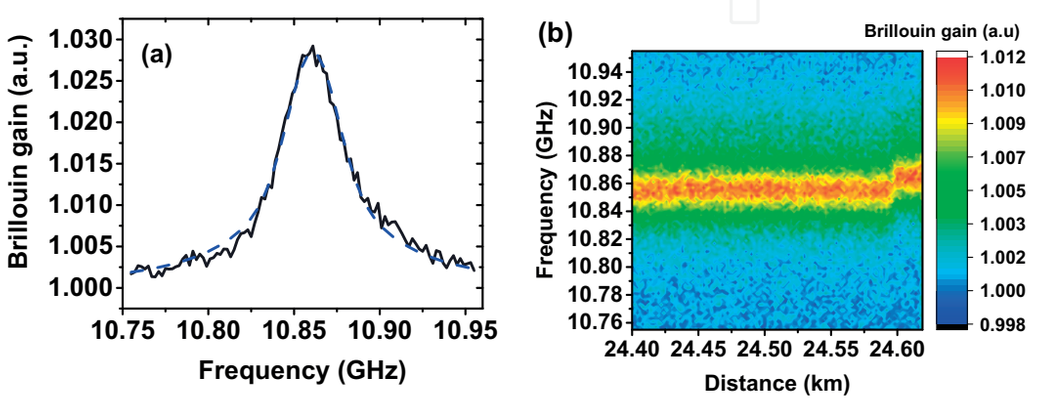

Figure 4.
(a) Measured BGS (solid) at a given fiber section with its Lorentzian fitting (dashed); (b) the reconstructed Brillouin gain mapping with a 20 m long hot spot at the fiber end.

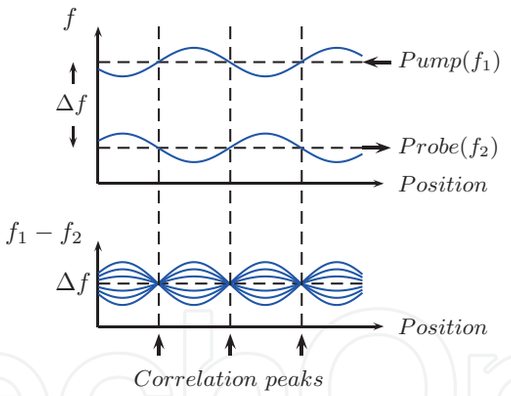

Figure 5.
Schematic explanation of BOCDA [48]. The frequency difference between pump and probe wave is constant at the correlation peaks.

nodes with the frequency difference properly set in the vicinity of the BFS of the FUT [48]. Since the frequency difference varies much faster than the time to excite an acoustic wave, only negligible Brillouin interactions will take place at the other positions. Therefore, unlike a pulse-based scheme such as BOTDA, the spatial resolution of a BOCDA system is usually high and determined by the modulation parameters (amplitude and frequency) written as:

$$\Delta z = \frac{v_g \cdot \nu_B}{2\pi f_m \cdot \Delta f} \tag{8}$$

where v_g is the group velocity, ν_B is the Brillouin gain linewidth, f_m and Δf are the modulation frequency and amplitude of the FM. By sweeping the frequency difference between the pump and probe wave, the BGS of the measured fiber position is scanned.

It is difficult to determine the contribution of the Brillouin interaction from multiple points of the fiber simultaneously. Therefore, the modulation frequency of both waves and the delay from one side should be carefully set, so that only a single correlation peak along the fiber is measured at a time. Thus, the sensing range of a BOCDA system is usually short and limited by the distance between adjacent correlation peaks $d_m = v_g/(2f_m)$. The location of the measured correlation peak can be shifted by changing the modulation frequency.

In comparison with other Brillouin sensing techniques, BOCDA has an excellent performance in achieving high spatial resolution, which depends on the FM modulation amplitude and the natural Brillouin linewidth. Besides, since the acoustic wave is excited by CW waves, the BGS linewidth will not be broadened. However, since each point along the fiber must be measured individually, the total measurement time will be linearly proportional to the amount of resolved points, which makes the measurement time also longer, compared to the other Brillouin sensing techniques.

3.2.4 BOFDA

The principle of the Brillouin optical frequency domain analyzer (BOFDA) [49] is based on the measurement of the complex transfer function that relates the amplitudes of the CW counterpropagating pump and probe wave with the FUT. The probe wave is frequency downshifted to the pump by the BFS and amplitude modulated with a sinusoidal function at a variable frequency. The modulated pump and probe wave intensities are measured at the end of the FUT with two separate photodiodes (PD) that fed to a network analyzer (NWA). By sweeping the modulation frequency, the NWA measures the baseband transfer function of the FUT,

whose inverse fast Fourier transformation approximates the pulse response of the FUT and represents the temperature and strain distribution. The high spatial resolution that BOFDA could achieve depends on the frequency sweep range, though, at the cost of the measurement time.

3.3 Basic setup of BOTDA

As illustrated in **Figure 6(a)**, a typical conventional BOTDA setup mainly comprises three parts. A highly coherent laser is split via a coupler into the probe (upper) and pump (lower) branch. A microwave signal, which can be scanned over the range of the BFS (~11 GHz ± 150 MHz), is applied on a Mach-Zehnder modulator (MZM 1) in the probe branch and biased in the carrier suppression regime. The generated lower frequency sideband serves as the probe wave, while the upper one is blocked by a narrow band-pass filter (FBG 1). The probe power is controlled by an erbium-doped fiber amplifier (EDFA 1) and launched into one end of the FUT. In the pump branch, the pump pulse with a required duration is formed by another MZM, amplified by EDFA 2 and launched into the other end of the fiber via a circulator (Cir 1). In order to mitigate the influence of the SBS polarization effect [50], the polarization of either pump or probe wave is scrambled via a polarization scrambler (Pol.S.) before launched into the fiber.

The Brillouin amplified probe wave is detected by a fast photodiode (PD) whose minimum bandwidth should correspond to the inverse of the pump pulse duration, to avoid any trace distortions. Another narrow band-pass filter (FBG 2) blocks the residual reflected pump wave. The electrical signal from the PD, which represents the evolution of the probe power, is processed digitally with a large number of averaging by a signal processor, that is, an oscilloscope or a digitizer. The Brillouin gain, which is essential for BFS estimation, can be derived by dividing the output of the PD by the probe power before the pump pulse is launched into the fiber [51].

3.4 Evaluation of the BOTDA performance

The BOTDA sensing performance is highly dependent on the estimation accuracy of the local BFS. According to recent investigations [52], system parameters such as the FWHM of the BGS $\Delta\nu_B$, the scanning frequency step δ, and the system noise σ, which is the inverse of the signal to noise ratio (SNR) of the normalized Brillouin gain, contribute significantly to an accurate estimation of a local BFS, as presented by the red curve in **Figure 6(b)**. Provided that $\nu_B(z)$ is the estimated BFS at distance z after a parabolic fitting of all experimental data above a given fraction η of the peak value (see **Figure 6(b)** for $\eta = 0.5$), the estimated error of the BFS is [52]:

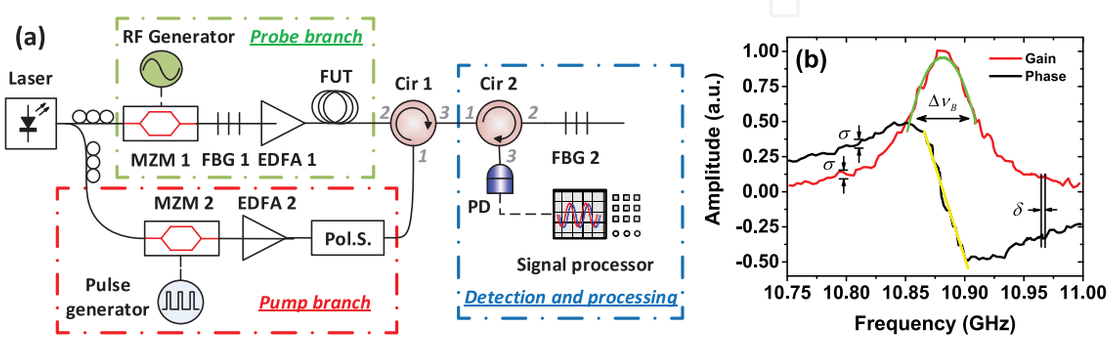

Figure 6.
(a) Conventional BOTDA setup. RF, radio frequency; MZM, Mach-Zehnder modulator; EDFA, erbium-doped fiber amplifier; Pol.S., polarization scrambler; FUT, fiber under test; PD, photodiode; Cir, circulator; FBG, fiber Bragg grating; (b) typical measured local BGS (red) and BPS (black) with system parameters that contribute to an uncertainty of the BFS estimation.

$$\sigma_V(z) = \sigma(z)\sqrt{\frac{3\cdot\delta\cdot\Delta\nu_B}{8\sqrt{2}(1-\eta)^{3/2}}} \underset{\eta=0.5}{\rightarrow} \sigma(z)\sqrt{\frac{3}{4}\delta\cdot\Delta\nu_B} = \frac{1}{SNR(z)}\sqrt{\frac{3}{4}\delta\cdot\Delta\nu_B} \tag{9}$$

As expected, a denser frequency sampling and a higher SNR value lead to a more accurate BFS estimation. Taking the relation of the SNR and number of averaging N_{AV} into consideration, that is, $SNR(z) \propto \sqrt{N_{AV}}$, the frequency error will also decrease significantly after thousands of averages due to an enhanced SNR. Owing to the linear dependence of the Brillouin phase response in the vicinity of the BFS, the sensor performance can also be evaluated by the linear fitting of the BPS [53] with a narrow frequency scanning and reduced measurement time (see black curve and yellow line in **Figure 6(b)**).

3.5 Major issues and limitations of BOTDA

3.5.1 Polarization fading

As discussed in Section 2.3, the Brillouin gain is highly dependent on the SOP of the pump and probe wave. Due to the weak birefringence of SMF, the SOP change of pump and probe leads to a highly nonuniform Brillouin gain along the fiber and consequently to a poor SNR for almost every fiber section, which is called polarization fading [50]. There are several solutions for polarization fading in a BOTDA system. The first proposed idea was to sequentially launch two orthogonal SOPs of the pump (or probe) wave and average the two measured results [4]. Another option is polarization scrambling, where the SOP of the pump and probe is varied rapidly so that the SOP is effectively randomized over time. It can be used in various scientific setups to cancel the errors caused by polarization-dependent effects. With a polarization scrambler and a digitizer, the traces can be averaged over thousands of pump pulses until a required high enough SNR is reached, though, at the cost of the BGS acquisition time.

3.5.2 Limitations on pump pulse width

According to the round-trip relation, the Brillouin interaction in a conventional BOTDA system takes place in a fiber section with a length of $cT/(2n)$, which can be seen as the spatial resolution [54], where c is the light speed in vacuum, n is the fiber refractive index and, T is the pulse duration. In principle, the spatial resolution could be enhanced by using shorter pulses. However, two main factors limit the spatial resolution to only 1 m.

First of all, decreasing the pulse duration will shorten the Brillouin interaction length and hence lower the SBS gain and consequently the SNR. Furthermore, the pump power spectrum for a shorter pulse will be severely broadened. Therefore, the resulting effective BGS should be modified as the convolution of the pump spectrum density and the natural Brillouin linewidth [21], that is,

$$g_B^{eff}(\nu) = g_B(\nu) \otimes I_p(\nu) \tag{10}$$

where $I_p(\nu)$ is the pump pulse power spectrum, which is significantly broadened to $1/T$ for pulses shorter than 20 ns [55]. The inherent broadening of the BGS leads to a decrease of the peak gain, which makes the estimation of the BGS peak more sensitive to the noise level. Moreover, it also indicates that the probe wave will be amplified only after the acoustic field is excited by the pump-probe interaction, which takes 10–30 ns. Due to the abovementioned reasons, the spatial resolution of

a conventional BOTDA system is limited to around 1 m, which corresponds to a pulse width of 10 ns.

3.5.3 Limitations on the pump wave power

In principle, the pump pulse power launched into the FUT should be high enough to compensate the fiber attenuation and hence generate an efficient Brillouin interaction. However, modulation instability (MI) in the optical fiber appears when the pulse power is beyond a certain threshold [56]. MI refers to the breakup of the balance between the anomalous dispersion and the Kerr effect, so that a train of soliton-like pulses rises from the noise as spectral sidebands symmetric to the pulse frequency [57, 58]. Several theoretical as well as experimental investigations have also demonstrated that there exists a periodical energy exchange between sidebands and pulse power along the fiber, that is, after a certain length of propagation, the pulse energy that has been spread to the sidebands will be transferred back to the pulse frequency and thus forms the Fermi-Pasta-Ulam recurrence [59].

For a conventional BOTDA system, this periodical power exchange leads to the fluctuation of the pump pulse power during the propagation and therefore distortions of the traces. As illustrated in **Figure 7(a)**, some of the fiber sections are not correctly interrogated due to the limited SNR. Furthermore, the critical power of the MI for a conventional BOTDA system with 25 km fiber is estimated to be as low as 135 mW [57]. Due to a rapid decrease of the Brillouin gain, MI severely limits the sensing range.

3.5.4. Limitations on the probe wave power

In order to achieve a high SNR for a better BFS estimation, a high enough probe wave power should be launched into the FUT. However, due to nonlocal effects (NLEs), the probe wave power in a conventional BOTDA system, that is, single probe sideband system, is usually limited to only −14 dBm [60]. The NLE generally refers to the fact that the Brillouin interaction from a local fiber segment is influenced by the interaction of other segments and hence leads to an error in the BFS estimation of the local fiber segment. It should be noticed that not only a too high probe power, but other factors, such as a limited pump pulse extinction ratio (ER), would also lead to NLE.

The origin of the NLE due to the high probe wave can well be explained by **Figure 7(b)** and the DES of SBS. As pointed out by Eq. (2) in Section 2.1, the

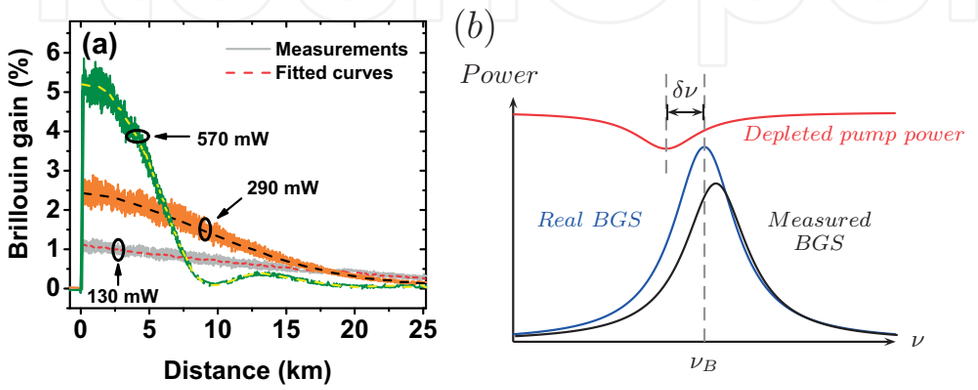

Figure 7.
(a) Distorted Brillouin traces due to MI with different input pump powers and fitted curves [57]. (b) Schematic explanation of the NLE due to the pump depletion in the FUT with uniform BFS in a long distance but nonuniform BFS in a distant section. δν is the frequency shift of BGS between the long uniform sections and the distant fiber segment [60].

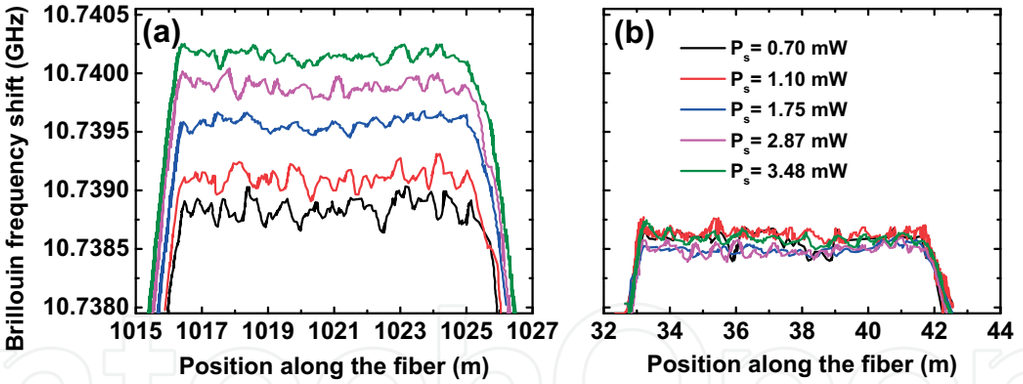

Figure 8.
BFS as a function of the position along the fiber when the hot spot is placed at (a) the far end and (b) the near end of the fiber for different signal (probe) powers P_s [60].

Brillouin interaction at each fiber segment not only amplifies the probe wave but also slightly depletes the pump power intensity. Since for each time-resolved interval, the CW probe wave interacts with the pump pulse only once, and the impact of the depletion becomes much higher on the pulse than on the probe wave. Therefore, the pump spectrum density is no longer independent of the Brillouin interaction that the pump pulse has experienced before reaching the distant fiber segment with nonuniform BFS (see **Figure 7(b)**). NLE typically leads to an asymmetry of the BGS and hence to an error in the BFS estimation. It should be noticed that, due to the accumulative impact of the depletion on the pump pulse, the NLE is in general more severe at the far end of the fiber (see **Figure 8**).

Another limitation on the probe power is the Brillouin threshold of the fiber. It is theoretically the maximum power that the input probe wave can have with no depletion and no thermally induced SpBS from the probe wave [61]. Since the Brillouin threshold is usually higher than the probe power limit due to the NLE, a series of techniques have to be applied to solve the NLE and then push the probe power limit toward the threshold of SBS.

4. State-of-the-art of BOTDA

As discussed in Section 3, due to the limitations on the pump pulse and probe power, the spatial resolution, and hence the sensing range and BFS measurement accuracy, a conventional BOTDA system is far from achieving an ideal performance. In order to compensate the SNR degradation, a higher averaging must be applied at the cost of measurement time. In this section, methods to break these limitations are reviewed.

The techniques introduced in this section are categorized according to their enhanced sensor performances. It is worth to notice that the contribution of each technique may lead to enhancements in several performances, for example, a technique that overcomes the MI enables a pump power higher than the limit and thus also an extended sensing range due to the increased Brillouin gain.

4.1 Strategies to avoid modulation instability

4.1.1 Noise filtering

The origin of MI is system noise, in which especially the amplified spontaneous emission (ASE) noise from the EDFA for pump pulse amplification plays an

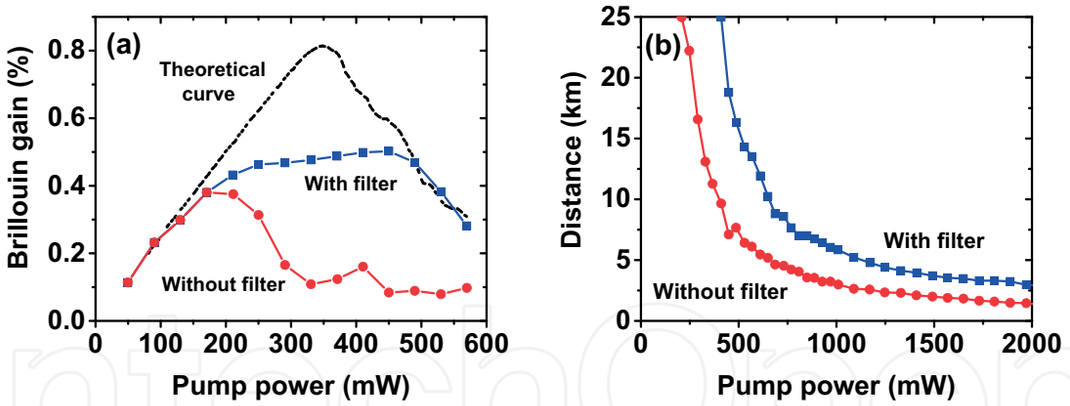

Figure 9.
Experimental results of the (a) Brillouin gain and (b) maximum distance (b) with an increasing input pump power with and without ASE noise filtering [62].

important factor. Therefore, a narrow band-pass optical filter after the pulse amplification might mitigate the MI [62]. Conventionally, the Brillouin gain is proportional to the input pump power, as indicated in **Figure 9(a)**. However, this is not the case if MI takes place. When the pump is depleted, the Brillouin gain decreases correspondingly. As indicated by the red line in **Figure 9(a)**, the application of the filter enables a slight increase of the Brillouin gain when the pump power is beyond the MI threshold, indicating a lower pump depletion in comparison to the case without the 1 GHz band-pass filter, and a mitigation of MI. Besides, the sensing range is also extended due to the lower pump depletion. **Figure 9(b)** illustrates experimental results for the distance that the pump pulse reaches when its amplitude is depleted by 50%. Since the MI extends over a band of ~60 GHz [62], it is believed that a filter wider than this bandwidth has a negligible contribution on the MI mitigation, while an enhanced mitigation is expected with a much narrower filter.

4.1.2 Dispersion-shifted fiber

Since the origin of MI is the interplay between the Kerr effect and anomalous dispersion, the MI can be eliminated in a dispersion-shifted fiber (DSF) with normal dispersion $D = -1.4$ ps/(nm·km) at 1550 nm [63]. As discussed in Section 3.5.3, the MI threshold in a 25 km SMF is estimated to be around 135 mW. However, as shown in **Figure 10(a)**, in DSF with the same length, no obvious trace distortion is observed at a pump pulse power of 400 mW, indicating a much higher MI threshold. An exponential fitting, which implies a pure fiber attenuation, further confirms the full

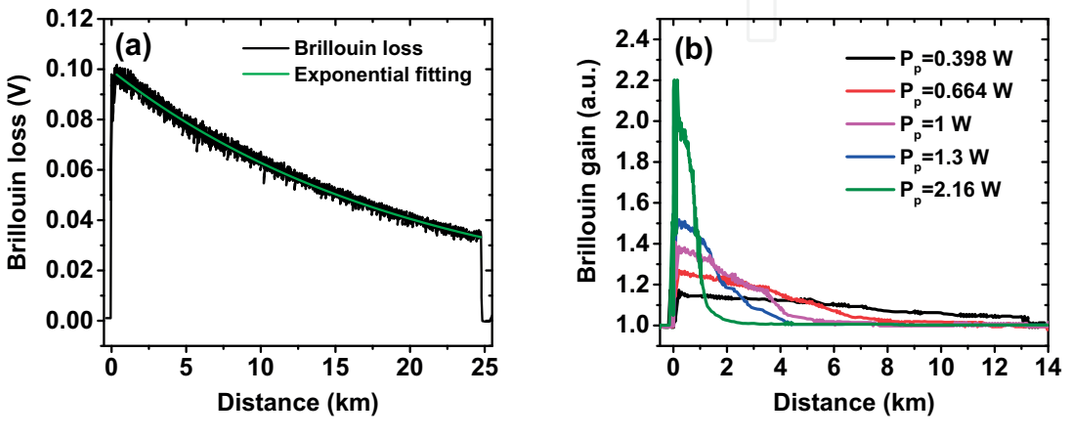

Figure 10.
(a) BOTDA trace in 25 km DSF with 400 mW pump power [63]; (b) distortions due to forward Raman scattering [64].

mitigation of MI. In comparison with other techniques, this technique is simple and requires no further change in the setup. However, DSFs of long length are much more costly than SMFs of the same length and DSFs usually have a higher attenuation.

Though the successful mitigation, according to a recent investigation [64], there are still pump power limitations. As shown in **Figure 10(b)**, for a pump pulse with a power of around 1 W, the traces are distorted mainly by forward Raman scattering.

4.1.3 Orthogonal polarized pump pulses

Since the single pump pulse power is limited by MI, a novel technique based on multiwavelength pumps was proposed to break the power limitation [65]. However, it has soon been identified that four wave mixing (FWM) between different spectral lines [65, 66] limits this approach. Thus, an orthogonal polarized dual-pump technique was proposed [67]. In this technique, two pump pulses with orthogonal SOP in different frequencies are launched into the FUT and interact with their corresponding probe waves. As shown in **Figure 11**, the orthogonal pumps effectively mitigate the MI in comparison with a single pump regime and successfully avoid the FWM interaction in comparison with the parallel polarized dual-pump regime both in time and frequency domain. It is worth to note that no additional polarization scrambler is required for orthogonal pulses, since two complementary Brillouin interactions are already ensured.

4.2 Strategies to avoid nonlocal effects

In an early proposal to avoid NLE, a general postprocessing algorithm was used for the BFS profile reconstruction [45]. Based on the BFS distribution that matches the measured data with a minimization algorithm in multidimensions, the parameters of the unknown BFS profile can be derived. However, the experimental realization complicates the setup and increases the processing time [68]. Another idea for the mitigation of NLE in general is to use pulses for both pump and probe wave [69]. However, despite the effective mitigation of the NLE, the shortened interaction length increases the measurement time significantly. In this subsection, other effective solutions for the NLE are reviewed.

4.2.1 Dual probe

One of the origins of NLE is the pump pulse depletion, which can be further separated in first- and second-order NLE. First-order NLEs are mainly caused by

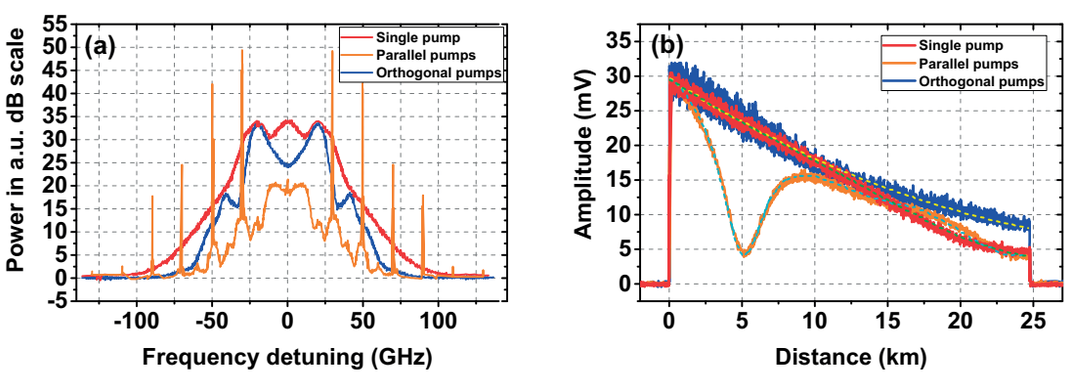

Figure 11.
(a) Simulated MI gain spectrum and (b) experimental time traces with single pump and parallel/orthogonal polarized dual-pump regime with ±10 GHz frequency detuning [67].

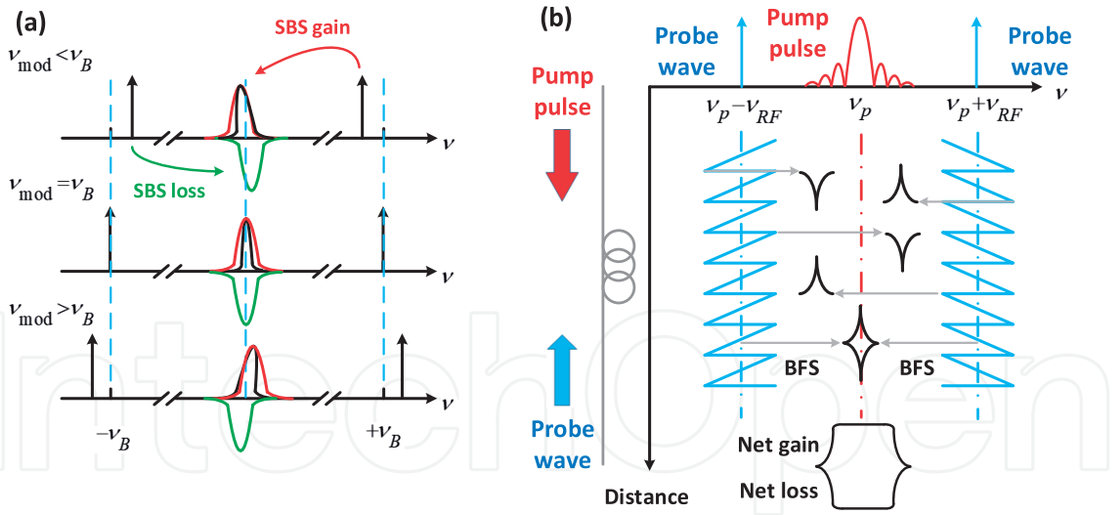

Figure 12.
Schematic explanation of (a) the Second-order NLE due to the distortion of the pump spectrum [70] and (b) the strategy to avoid it using an FM probe wave [73].

pump depletion due to a high probe power. Second-order NLEs are based on linear distortions of the pump pulse spectrum. Second-order NLEs can even happen when first-order NLEs are completely mitigated [70].

The most popular solution for first-order NLE mitigation is the dual-probe sideband regime. In contrast to a conventional BOTDA system, both probe wave sidebands generated by the MZM are involved in the SBS interaction. The pump pulse depletion due to the energy transfer to the lower frequency sideband is compensated by an energy transfer from the upper frequency sideband to the pump. A theoretical analysis reveals that in the dual-probe sideband regime, the probe power limit rises from −14 to −3 dBm [60, 71]. Furthermore, since the energy transfer from the high power (pump) to the low power (probe) is more efficient than the reverse process, slightly unbalanced dual-probe sidebands mitigate NLE better than balanced ones [60, 72].

Even with dual probe regime, second-order NLEs still exist [70]. This kind of NLE has its origin not in the depleted pump, but in the frequency-dependent distortion of the pump pulse spectrum that affects the interaction in the gain and loss configuration differently (see **Figure 12(a)**). However, a total mitigation of first- and second-order NLEs can be achieved with dual-probe sidebands [61] with additional FM in saw-tooth shape [73]. A similar performance enhancement can also be achieved with sinusoidal or a triangular shape [61, 74]. If the FM is synchronized to the pump pulses (see **Figure 12(b)**), a series of pulses at a specific fiber position interacts always with the same probe frequency. In turn, each single pulse experiences SBS interactions with probe waves that have different frequency detunings as it propagates along the fiber. Since the pulse depletion is accumulated along the fiber, a decreased distortion upon the pulse spectrum can be achieved by interacting with different frequencies within the BGS, indicating a mitigation of the second-order NLE. Together with the mitigation of the first-order NLE by dual-probe sidebands regime, the probe power limit has been successfully pushed to a record of 8 dBm [61], reaching the Brillouin threshold of SMF in ~20 km range.

4.2.2 Higher pulse extinction ratio

Another origin of NLE is the imperfect pulsing of the pump wave. Due to the limited extinction ratio (ER) of common pulsing methods, there is a residual power leakage. Since the pulse pedestals have the same frequency as the pump, SBS

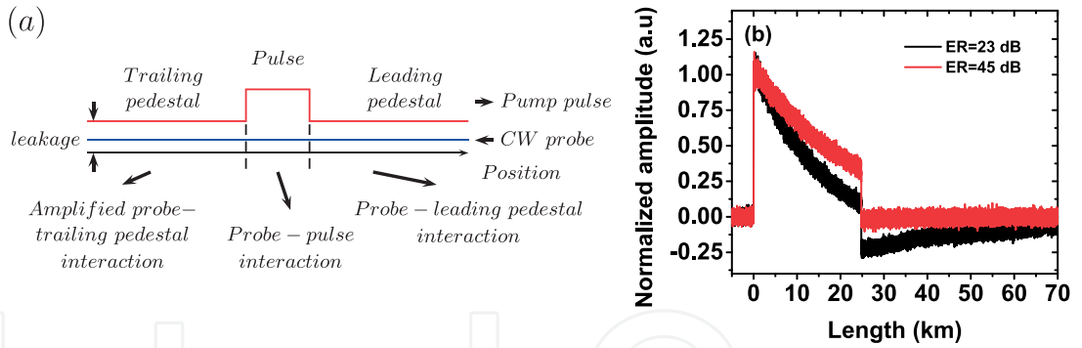

Figure 13.
(a) The schematic description of the interaction between pulse and probe wave [75]; (b) the distorted BOTDA traces under different pulse ER due to the pump pedestal depletion [76].

interactions can take place between the probe wave and the leading as well as the trailing pedestals [75], as schematically depicted in **Figure 13(a)**. Therefore, the net effect of the presence of the pulse pedestal is that the probe wave will be additionally amplified. However, this amplification is not useful for sensing. In case of a strong probe wave, not only the pulse but also the pedestals (especially the trailing pedestal) will deplete, which lead to severe distortions on the BOTDA traces (see **Figure 13(b)**) [75, 76].

Under a very low ER, the interactions between probe wave and pedestals may dominate the final BGS detection due to a long interaction length and leads to an error on the BFS estimation (see **Figure 14(a)** and **(b)**) [77]. For a conventional MZM, the ER is only 20 dB but can be enhanced up to 30 dB with special designs. Higher ERs of more than 40 dB can be achieved with switching type semiconductor optical amplifiers (SOA) and a 60 dB ER with RF switches [75, 76].

4.3 Enhancement of the spatial resolution

4.3.1 Differential pulse width pair (DPP)

In a DPP-BOTDA system, two consecutive measurements are carried out with the same pulse peak power but slightly different durations, T and $T + \Delta T$. Usually, T is longer than the phonon excitation time, indicating a full excitation of the acoustic wave in both measurements and ΔT is short so as to achieve a high spatial resolution [78]. Since both pump pulses give the same amplification in the time slot T and only the longer pulse contributes amplification in the extra time ΔT, the subtraction of the two measured Brillouin amplified probe signals yields to the BGS in the time slot ΔT.

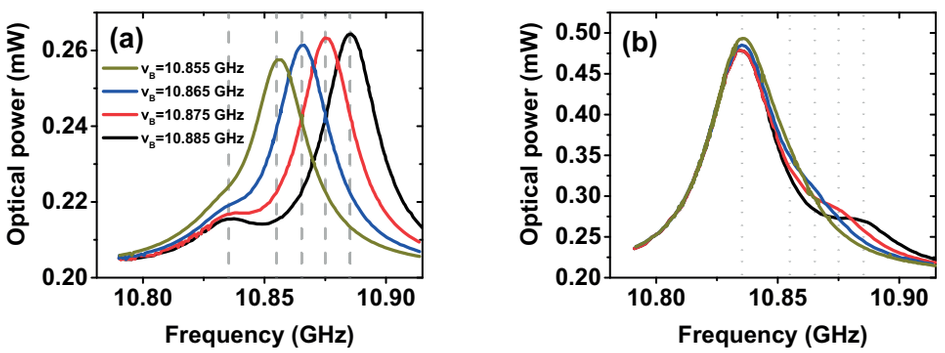

Figure 14.
The simulation of the BGS with pump pulse of (a) ER = 40 dB and (b) ER = 26 dB at the hot spots in different temperatures (different BFSs). The uniform BFS of the rest of the fiber is ν_{B0} = 10.835 GHz [77].

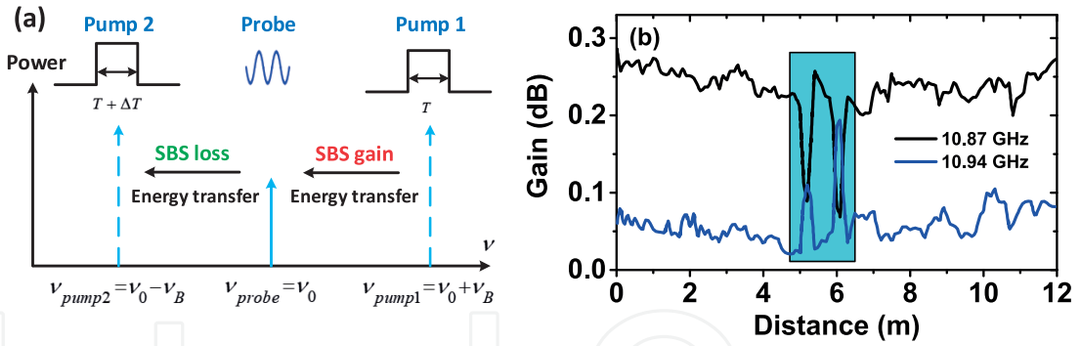

Figure 15.
(a) Schematic description of the simultaneous DPP-BOTDA in the frequency domain and (b) Brillouin gain profile in the experiment. Along the fifth meter of the fiber, two 20 cm fiber sections were located 65 cm apart and manually stretched to have nonuniform strains [79].

Later on, the DPP-BOTDA technique has been developed into a simultaneous measurement by launching two pump pulses with slightly different durations in different frequencies [79]. Pump pulse 1 with duration T interacts with the probe wave via SBS loss, while simultaneously pump pulse 2 with duration $T + \Delta T$ interacts with the probe wave via SBS gain (see **Figure 15(a)**). Therefore the subtraction of the BGS is automatically achieved at the detector with no postprocessing required. A 10 cm spatial resolution BOTDA system has been reported by using a 30 ns gain pump pulse and a 29 ns loss pump pulse (see **Figure 15(b)**) [79]. However, in comparison with the pre-excitation method, the subtraction of the traces adds noise to the data. Therefore, in order to achieve the required SNR, massive averaging must be applied.

4.3.2 Pre-excitation

The reason for the spatial resolution limit of around 1 m is the excitation time of the phonon. A prepump excitation can solve this problem by shaping the pump pulse into two parts, that is, a long pedestal with low power (prepump pulse (PPP), part 1 in **Figure 16(a)**) for the phonon excitation, followed by a narrow high power pulse (part 2 in **Figure 16(a)**) [80]. In order to excite the phonon, the PPP is usually longer than 10 ns. To achieve high spatial resolutions, the high power pulse can be very short (~1 ns). **Figure 16(b)** shows experimental results when the PPP (12 ns duration), the high power pulse (1 ns duration), and the total pump pulse interrogate a 20 cm fiber section with strain individually. The resulting BGS of the total

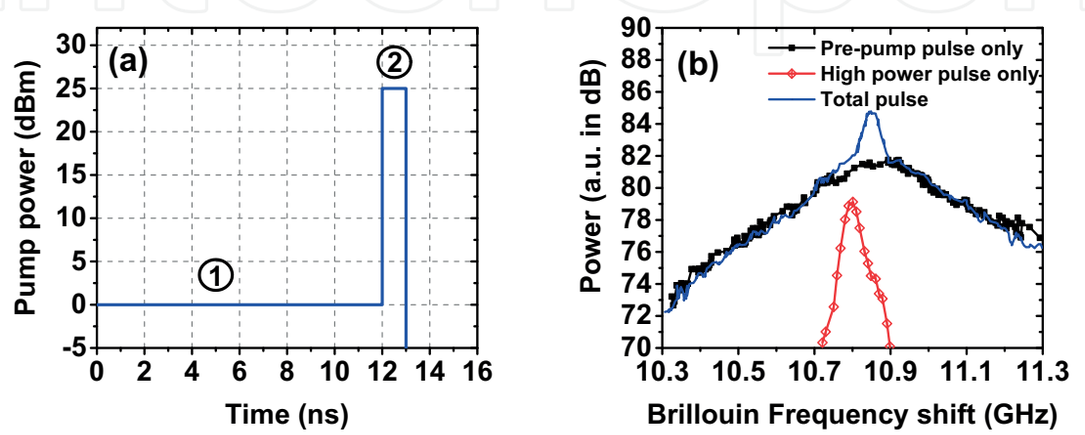

Figure 16.
(a) Pulse shape for pre-excitation technique; (b) BGS of a fiber section with strain interrogated by the PPP only (red), high power pulse only (black), and total pulse (blue) [80].

pulse is characterized by a broadened spectrum with low amplitude and a narrow cap, whose width is determined by the high power pulse and PPP, respectively. A clear BFS shift between the PPP and total pulse case indicates an enhancement of the spatial resolution down to ~10 cm. In comparison to DPP-BOTDA, the high spatial resolution by pre-excitation does not come at the expense of a decreased SNR and therefore, it is more favorable for commercial use.

4.4 Enhancement of the sensing range

Due to the fiber attenuation or other depletions, the sensing range of a conventional BOTDA system is usually limited by the low SNR at the far end of the fiber to only a few tens of kilometers [51]. Therefore, the key to extend the sensing range is either to enhance the probe signal power or to eliminate the system noise.

4.4.1 Multi-frequency pump-probe interaction

In this technique, the total pump power is spread over multiple-pump waves in different frequencies, with every single pump power still limited by MI [65]. The theoretical enhancement of the SNR could reach the number of pumps N. However, severe FWM occurs for too narrow pump frequency spacing, while the BGS linewidth from each pump may differ when they are too widely separated apart [65]. The solution for the latter is a postprocessing algorithm [81], while the solution to avoid the FWM is to shift the pump pulse propagation in time domain with a frequency-selective time shifter, which can be realized by N-consecutive FBGs separated by a certain length of fiber in the experiment. The schematic description of the frequency-selective time shifter is illustrated in **Figure 17(a)**. After the time-shifted pump pulses have interacted with their corresponding probe waves, another consecutive FBG with a reversed sequence offers a reversed delay and combines the traces back in time domain so that they can be simultaneously detected. For a three pump system, an SNR improvement of 4.8 dB has been demonstrated (see **Figure 17(b)**) [65].

4.4.2 Self-heterodyne detection

Another possibility to amplify the signal amplitude is the heterodyne detection. Provided that the Brillouin amplified probe wave at frequency ν_s beats with an local oscillator at frequency ν_{LO}, the total electrical field can be expressed as [30]:

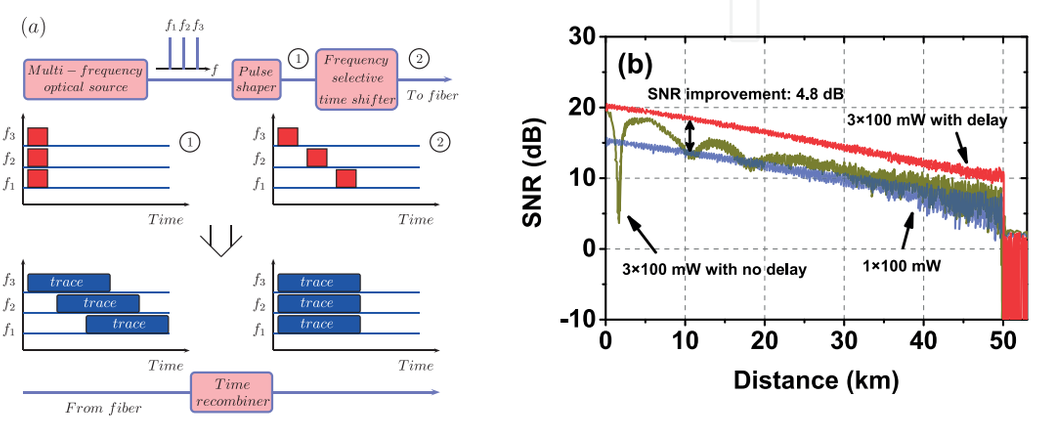

Figure 17.
(a) Schematic explanation of the time shifter and recombiner; (b) SNR measured in the experiment for standard BOTDA (single pulse), three pulses with and without time delay [65].

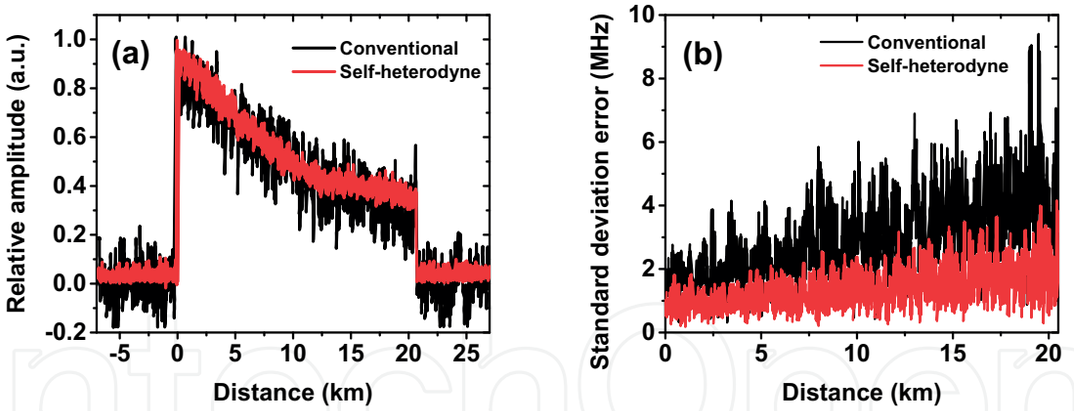

Figure 18.
(a) BOTDA traces and (b) BFS standard deviation of consecutive measurements with (red) and without (black) self-heterodyne detection [30].

$$E_T(t,\nu) = E_{S0}\, g_{SBS}(\nu_s, z) \exp\{j \cdot [2\pi\nu_s t + \phi_{SBS}(\nu_s, z)]\} + E_{LO} \exp(j \cdot 2\pi\nu_{LO} t) \quad (11)$$

where E_{s0} and E_{LO} are the complex amplitude of the probe wave and local oscillator, g_{SBS} and ϕ_{SBS} are the SBS gain and phase shift. Hence, the detected current at the PD can be written as:

$$I_c(t) = R_c P_T = 2R_C \sqrt{P_{s0}\left[1 + g_{SBS}(\nu_s, z)\right]^2 P_{LO}} \cdot \cos\left[2\pi f_{IF} t + \phi_0 - \phi_{SBS}(\nu_s, z)\right] \quad (12)$$

where ϕ_0 and f_{IF} are the phase and frequency difference between the probe wave and local oscillator, P_{LO} and P_{S0} are the optical power of the local oscillator and probe wave, R_c is the PD responsivity. As the detected current is dependent on the power of the local oscillator, the whole mechanism could be regarded as a signal amplification with a strong oscillator. As shown in **Figure 18(a)**, the trace detected by self-heterodyne is cleaner and has an SNR enhancement of 10 dB [30]. Further investigations with five consecutive distributed measurements show that the self-heterodyne detection decreases also the BFS standard deviation (see **Figure 18(b)**), indicating a more accurate BFS estimation. In comparison with other techniques, self-heterodyne detection provides the most simple and feasible scheme for sensing range enhancement.

4.5 Enhancement on measurement time

For a conventional BOTDA, it usually takes several minutes to finish a single measurement, which is impractical for dynamic strain sensing. One of the main factors that limit the measurement time is the sweeping of the probe frequency to scan the total BGS. Therefore, several techniques have been applied to solve this problem.

4.5.1 Slope-assisted BOTDA

One of the techniques for dynamic sensing is based on partially scanning the BGS [82]. In order to achieve the BGS profile in general, the technique requires a preliminary frequency scan without vibration. The probe scanning frequency is then set at half of the BGS linewidth, as shown in **Figure 19(a)**. This 3 dB point has the steepest slope and widest linear range and is the most sensitive working point for tiny frequency shifts. The BGS is reconstructed according to the measured signal amplitude, and the strain values are obtained by the strain coefficient C_ε mentioned

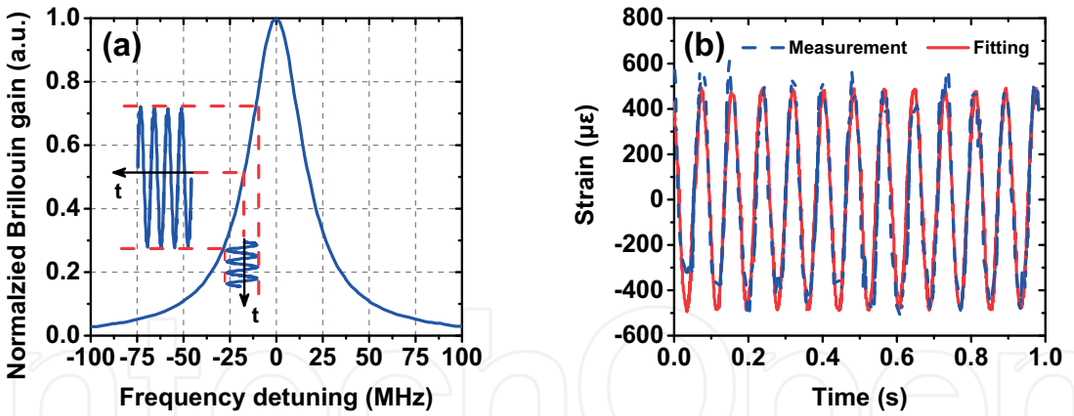

Figure 19.
(a) Schematic explanation of the dynamic sensing with the working point set at the half value of the peak Brillouin gain and (b) dynamic strain measurement based on this technique [82].

in Section 3.1. In **Figure 19(b)**, the proposed technique is demonstrated with a perturbation frequency of 12.3 Hz. Obviously, this technique can only detect small temperature or strain distributions and is not applicable for a BFS nonuniformity that exceeds half of the BGS linewidth.

4.5.2 Sweep-free multi-tones

Another idea to speed up the measurement time is to utilize multitone pumps [66]. As shown in **Figure 20(a)**, multiple pumps with multiple frequencies are launched into the fiber aligning at different frequency detunings of the BGSs. Since the multi-SBS interactions happen simultaneously, the necessary frequency sweeping can be done in a single shot. Thus, the total measurement time including extra averaging measurements for SNR improvement lasts only several seconds.

However, there are still trade-offs and limitations in this technique. Undesired FWM occurs when the pump pulses are simultaneously launched. This can be solved by unequal spacing or a sequential launch of the pumps. The total number of pump tones, which determines the accuracy of the BGS reconstruction, is restricted by the intertone spacing Δf and the total tone span f_{total}. The intertone spacing is usually larger than the total BGS width so as to avoid BGS overlaps. The total tone span should not exceed the BFS so that no pump lines are within the BGS of other pumps.

Recently, a new improved method has been proposed to avoid these limitations by utilizing digital optical frequency combs (DOFC) as probe signals [83]. Since the probe wave power in the BOTDA system is usually low, multiple-probe waves suffer less from FWM than multiple pumps. The DOFC owns narrow frequency spacing, wide flat top, and total bandwidth, as depicted in **Figure 20(b)**. According

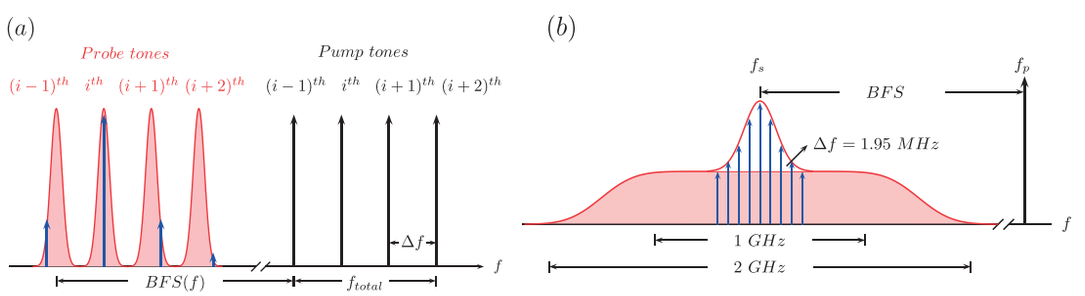

Figure 20.
(a) Schematic explanation of the principle of the sweep-free multitone BOTDA [81]; (b) spectrum of DOFC [83].

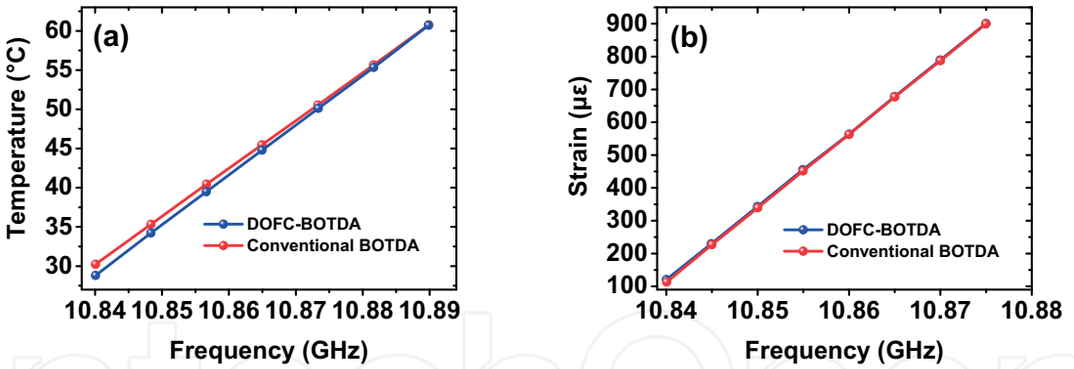

Figure 21.
The linear fitting of (a) temperature and (b) strain measurement with conventional BOTDA and DOFC-BOTDA [83].

to the frequency difference between each line and the pump frequency, the pump pulse shapes the amplitude of each spectral comb line via the SBS interaction simultaneously. The total measurement time, including the necessary 100 acquisitions for the SNR improvement, results in only 10 ms [83]. Furthermore, the experimental results in **Figure 21** confirm its equivalence to a conventional BOTDA regarding the temperature and strain measurement. However, the main disadvantage of this technique is the special requirement of the DOFC, which is generally not so simple to achieve.

5. Summary

In this chapter, the basics of SBS and its application for distributed sensing have been reviewed. The overview has started with an introduction of SBS together with its physical origin and applications due to inherent, striking advantages in a variety of fields such as slow light, optical and microwave photonic filters, and many more. Among all these exciting applications, distributed temperature and strain sensing is one of the most prominent.

The enhanced SNR and the moderate resolution are the superiority of distributed Brillouin sensors to the traditional distributed and point sensors in long-range sensing. However, conventional BOTDA sensors are limited by MI and NLE. The origins, as well as methods for the mitigation of MI and NLE, have been presented and discussed in detail. Thus, with these new methods, much longer sensing ranges became possible.

Besides the sensing range, methods to enhance the spatial resolution and the speed of the measurement have also been reviewed and discussed. Nowadays, distributed Brillouin fiber sensors can have a resolution in the centimeter range, or even below and act like thousands or millions of point sensors. At the same time, novel ideas such as multi-tone pumps have successfully shortened the measurement time in distributed SBS sensors from several minutes down to ~10 ms. Due to the fruitful proof-of-concept results, some of the state-of-the-art techniques discussed in this chapter have already been applied in some BOTDA prototypes.

Acknowledgements

Cheng Feng wishes to acknowledge the financial support from German Research Foundation (DFG SCHN 716/13-1) and Niedersächsisches Vorab (NL—4 Project

"QUANOMET"). Jaffar Emad Kadum would like to acknowledge the financial support of Iraqi Ministry of Oil/State Company for Oil Projects (SCOP).

Author details

Cheng Feng*, Jaffar Emad Kadum and Thomas Schneider
Institute for High Frequency Technology, Technical University of Braunschweig, Braunschweig, Germany

*Address all correspondence to: cheng.feng@ihf.tu-bs.de

References

[1] López-Higuera JM, editor. Handbook of Optical Fibre Sensing Technology. Chichester: Wiley; 2002

[2] Barnoski MK, Rourke MD, Jensen SM, Melville RT. Optical time domain reflectometer. Applied Optics. 1977;**16**: 2375-2379. DOI: 10.1364/AO.16.002375

[3] Grattan KTV, Sun T. Fiber optic sensor technology: An overview. Sensors and Actuators A: Physical. 2000;**82**:40-61. DOI: 10.1016/S0924-4247(99)00368-4

[4] Horiguchi T, Tateda M. Optical-fiber-attenuation investigation using stimulated Brillouin scattering between a pulse and a continuous wave. Optics Letters. 1989;**14**:408-410. DOI: 10.1364/OL.14.000408

[5] Brillouin L. Diffusion de la lumière et des rayons X par un corps transparent homogène. Annals of Physics. 1922;**9**: 88-122. DOI: 10.1051/anphys/192209170088

[6] Ippen EP, Stolen RH. Stimulated Brillouin scattering in optical fibers. Applied Physics Letters. 1972;**21**: 539-541. DOI: 10.1063/1.1654249

[7] Agrawal GP. Nonlinear Fiber Optics. 5th ed. Amsterdam: Elsevier, Academic Press; 2013

[8] Shelby RM, Levenson MD, Bayer PW. Guided acoustic-wave Brillouin scattering. Physical Review B. 1985;**31**: 5244-5252. DOI: 10.1103/PhysRevB.31.5244

[9] Antman Y, London Y, Zadok A. Scanning-free characterization of temperature dependence of forward stimulated Brillouin scattering resonances. In: Kalinowski HJ, Fabris JL, Bock WJ, editors. 24th Int. Conf. Opt. Fibre Sensors. Vol. 9634. 2015. p. 96345C. DOI: 10.1117/12.2195097

[10] Antman Y, Clain A, London Y, Zadok A. Optomechanical sensing of liquids outside standard fibers using forward stimulated Brillouin scattering. Optica. 2016;**3**:510. DOI: 10.1364/OPTICA.3.000510

[11] Boyd RW. Nonlinear Optics. 3rd ed. Singapore: Elsevier; 2008

[12] Smith RG. Optical power handling capacity of low loss optical fibers as determined by stimulated Raman and Brillouin scattering. Applied Optics. 1972; **11**:2489. DOI: 10.1364/AO.11.002489

[13] Küng A. Laser Emission in Stimulated Brillouin Scattering in Optical Fiber. Lausanne, Switzerland: Ecole Polytechnique Fédérale de Lausanne; 1997

[14] Bayvel P, Radmore PM. Solutions of the SBS equations in single mode optical fibres and implications for fibre transmission systems. Electronics Letters. 1990;**26**:434. DOI: 10.1049/el:19900282

[15] Le Floch S, Cambon P. Theoretical evaluation of the Brillouin threshold and the steady-state Brillouin equations in standard single-mode optical fibers. Journal of the Optical Society of America. A. 2003;**20**:1132. DOI: 10.1364/JOSAA.20.001132

[16] Engelbrecht R. Analysis of SBS gain shaping and threshold increase by arbitrary strain distributions. Journal of Lightwave Technology. 2014;**32**: 1689-1700. DOI: 10.1109/JLT.2014.2310214

[17] Zadok A, Eyal A, Tur M. Stimulated Brillouin scattering slow light in optical fibers [invited]. Applied Optics. 2011; **50**:E38. DOI: 10.1364/AO.50.000E38

[18] Wei W, Yi L, Jaouën Y, Hu W. Bandwidth-tunable narrowband rectangular optical filter based on

stimulated Brillouin scattering in optical fiber. Optics Express. 2014;**22**: 23249-23260. DOI: 10.1364/OE.22.023249

[19] Feng C, Preussler S, Schneider T. Sharp tunable and additional noise-free optical filter based on Brillouin losses. Photonics Research. 2018;**6**:132-137. DOI: 10.1364/PRJ.6.000132

[20] Stern Y, Zhong K, Schneider T, Zhang R, Ben-Ezra Y, Tur M, et al. Tunable sharp and highly selective microwave-photonic band-pass filters based on stimulated Brillouin scattering. Photonics Research. 2014;**2**:B18-B25. DOI: 10.1364/PRJ.2.000B18

[21] Zhu Z, Dawes AM, Gauthier DJ, Zhang L, Willner AE. 12-GHz-bandwidth SBS slow light in optical fibers. In: Opt. Fiber Commun. Conf.; Optical Society of America. 2006. p. PDP1

[22] Schneider T, Junker M, Lauterbach K-U. Potential ultra wide slow-light bandwidth enhancement. Optics Express. 2006;**14**:11082-11087. DOI: 10.1364/OE.14.011082

[23] Schneider T, Henker R, Lauterbach K-U, Junker M. Adapting Brillouin spectrum for slow light delays. Electronics Letters. 2007;**43**:682. DOI: 10.1049/el:20070313

[24] Preussler S, Wiatrek A, Jamshidi K, Schneider T. Brillouin scattering gain bandwidth reduction down to 3.4 MHz. Optics Express. 2011;**19**:8565-8570. DOI: 10.1364/OE.19.008565

[25] Wiatrek A, Preußler S, Jamshidi K, Schneider T. Frequency domain aperture for the gain bandwidth reduction of stimulated Brillouin scattering. Optics Letters. 2012;**37**: 930-932. DOI: 10.1364/OL.37.000930

[26] Preussler S, Schneider T. Bandwidth reduction in a multistage Brillouin system. Optics Letters. 2012;**37**: 4122-4124. DOI: 10.1364/OL.37.004122

[27] Preussler S, Schneider T. Stimulated Brillouin scattering gain bandwidth reduction and applications in microwave photonics and optical signal processing. Optical Engineering. 2016;**55**:031110. DOI: 10.1117/1.OE.55.3.031110

[28] Preussler S, Wiatrek A, Jamshidi K, Schneider T. Quasi-light-storage enhancement by reducing the Brillouin gain bandwidth. Applied Optics. 2011;**50**: 4252-4256. DOI: 10.1364/AO.50.004252

[29] Feng C, Preussler S, Schneider T. The influence of dispersion on stimulated Brillouin scattering based microwave photonic notch filters. Journal of Lightwave Technology. 2018; **36**:5145-5151. DOI: 10.1109/JLT.2018.2871037

[30] Zornoza A, Sagues M, Loayssa A. Self-heterodyne detection for SNR improvement and distributed phase-shift measurements in BOTDA. Journal of Lightwave Technology. 2012;**30**: 1066-1072. DOI: 10.1109/JLT.2011.2168808

[31] Horiguchi T, Shibata N, Azuma Y, Tateda M. Brillouin gain variation due to a polarization-state change of the pump or stokes fields in standard single-mode fibers. Optics Letters. 1989;**14**:329. DOI: 10.1364/OL.14.000329

[32] Sharma GP, Preubler S, Schneider T. Precise optical frequency shifting using stimulated Brillouin scattering in optical Fibers. IEEE Photonics Technology Letters. 2017;**29**:1467-1470. DOI: 10.1109/LPT.2017.2729598

[33] Al-Taiy H, Wenzel N, Preußler S, Klinger J, Schneider T. Ultra-narrow linewidth, stable and tunable laser source for optical communication systems and spectroscopy. Optics Letters. 2014;**39**:5826-5829. DOI: 10.1364/OL.39.005826

[34] Preussler S, Zadok A, Wiatrek A, Tur M, Schneider T. Enhancement of spectral resolution and optical rejection ratio of Brillouin optical spectral analysis using polarization pulling. Optics Express. 2012;**20**:14734-14745. DOI: 10.1364/OE.20.014734

[35] Preussler S, Schneider T. Attometer resolution spectral analysis based on polarization pulling assisted Brillouin scattering merged with heterodyne detection. Optics Express. 2015;**23**: 26879-26887. DOI: 10.1364/OE.23.026879

[36] Preussler S, Wenzel N, Schneider T. Flat, rectangular frequency comb generation with tunable bandwidth and frequency spacing. Optics Letters. 2014; **39**:1637-1640. DOI: 10.1364/OL.39.001637

[37] Preußler S, Wenzel N, Braun R-P, Owschimikow N, Vogel C, Deninger A, et al. Generation of ultra-narrow, stable and tunable millimeter- and terahertz-waves with very low phase noise. Optics Express. 2013;**21**:23950-23962. DOI: 10.1364/OE.21.023950

[38] Preussler S, Wenzel N, Zadok A, Schneider T. Tunable generation of ultra-narrow linewidth millimeter and THz-waves and their modulation at 40 Gbd. In: 2013 IEEE Int. Top. Meet. Microw. Photonics. IEEE; 2013. pp. 119-122. DOI: 10.1109/MWP.2013.6724034

[39] Timoshenko S, Goodier J. Theory of Elasticity. New York: McGraw-Hill; 1970

[40] Kurashima T, Tateda M. Thermal effects on the Brillouin frequency shift in jacketed optical silica fibers. Applied Optics. 1990;**29**:2219-2222. DOI: 10.1364/AO.29.002219

[41] Horiguchi T, Kurashima T, Tateda M. Tensile strain dependence of Brillouin frequency shift in silica optical fibers. IEEE Photonics Technology Letters. 1989;**1**:107-108. DOI: 10.1109/68.34756

[42] Galindez-Jamioy CA, López-Higuera JM. Brillouin distributed fiber sensors: An overview and applications. Journal of Sensors. 2012;**2012**:1-17. DOI: 10.1155/2012/204121

[43] Zou W, He Z, Kishi M, Hotate K. Stimulated Brillouin scattering and its dependences on strain and temperature in a high-delta optical fiber with F-doped depressed inner cladding. Optics Letters. 2007;**32**:600. DOI: 10.1364/OL.32.000600

[44] Zou W, He Z, Hotate K. Investigation of strain- and temperature-dependences of Brillouin frequency shifts in GeO2-doped optical fibers. Journal of Lightwave Technology. 2008;**26**:1854-1861. DOI: 10.1109/JLT.2007.912052

[45] Bernini R, Minardo A, Zeni L. Reconstruction technique for stimulated Brillouin scattering distributed fiber-optic sensors. Optical Engineering. 2002;**41**:2186-2194. DOI: 10.1117/1.1497176

[46] Kurashima T, Horiguchi T, Izumita H, Furukawa S, Koyamada Y. Brillouin optical-fiber time domain reflectometry. IEICE Transactions on Communications. 1993;**E76-B**:382-390

[47] Song K-Y, He Z, Hotate K. Distributed strain measurement with Millimeter-order spatial resolution based on Brillouin optical correlation domain analysis and beat lock-in detection scheme. In: Opt. Fiber Sensors. Washington, D.C.: OSA; 2006. p. ThC2. DOI: 10.1364/OFS.2006.ThC2

[48] Song K-Y, Hotate K. Brillouin optical correlation domain analysis in linear configuration. IEEE Photonics Technology Letters. 2008;**20**:2150-2152. DOI: 10.1109/LPT.2008.2007744

[49] Garus D, Krebber K, Schliep F, Gogolla T. Distributed sensing technique based on Brillouin optical-fiber frequency-domain analysis. Optics Letters. 1996;**21**:1402-1404. DOI: 10.1364/OL.21.001402

[50] Zadok A, Zilka E, Eyal A, Thévenaz L, Tur M. Vector analysis of stimulated Brillouin scattering amplification in standard single-mode fibers. Optics Express. 2008;**16**:21692-21707. DOI: 10.1364/OE.16.021692

[51] Motil A, Bergman A, Tur M. State of the art of Brillouin fiber-optic distributed sensing. Optics and Laser Technology. 2016;**78**:81-103. DOI: 10.1016/j.optlastec.2015.09.013

[52] M a S, Thévenaz L. Modeling and evaluating the performance of Brillouin distributed optical fiber sensors. Optics Express. 2013;**21**:31347-31366. DOI: 10.1364/OE.21.031347

[53] Lopez-Gil A, Soto MA, Angulo-vinuesa X, Dominguez-Lopez A, Martin-Lopez S, Thévenaz L, et al. Evaluation of the accuracy of BOTDA systems based on the phase spectral response. Optics Express. 2016;**24**: 17200-17214. DOI: 10.1364/OE.24.017200

[54] Horiguchi T, Shimizu K, Kurashima T, Tateda M, Koyamada Y. Development of a distributed sensing technique using Brillouin scattering. Journal of Lightwave Technology. 1995; **13**:1296-1302. DOI: 10.1109/50.400684

[55] Lecoeuche V, Webb DJ, Pannell CN, D a J. Transient response in high-resolution Brillouin-based distributed sensing using probe pulses shorter than the acoustic relaxation time. Optics Letters. 2000;**25**:156. DOI: 10.1364/OL.25.000156

[56] Tai K, Hasegawa A, Tomita A. Observation of modulational instability in optical fibers. Physical Review Letters. 1986;**56**:135-138. DOI: 10.1103/PhysRevLett.56.135

[57] Alem M, Soto MA, Thévenaz L. Analytical model and experimental verification of the critical power for modulation instability in optical fibers. Optics Express. 2015;**23**:29514-29532. DOI: 10.1364/OE.23.029514

[58] Tai K, Tomita A, Jewell JL, Hasegawa A. Generation of subpicosecond solitonlike optical pulses at 0.3 THz repetition rate by induced modulational instability. Applied Physics Letters. 1986;**49**:236-238. DOI: 10.1063/1.97181

[59] Van Simaeys G, Emplit P, Haelterman M. Experimental demonstration of the Fermi-Pasta-Ulam recurrence in a modulationally unstable optical wave. Physical Review Letters. 2001;**87**:033902. DOI: 10.1103/PhysRevLett.87.033902

[60] Thévenaz L, Mafang SF, Lin J. Effect of pulse depletion in a Brillouin optical time-domain analysis system. Optics Express. 2013;**21**:14017-14035. DOI: 10.1364/OE.21.014017

[61] Ruiz-Lombera R, Urricelqui J, Sagues M, Mirapeix J, López-Higuera JM, Loayssa A. Overcoming nonlocal effects and Brillouin threshold limitations in Brillouin optical time-domain sensors. IEEE Photonics Journal. 2015;**7**. DOI: 10.1109/JPHOT.2015.2498543

[62] Soto MA, Alem M, Chen W, Thévenaz L. Mitigating modulation instability in Brillouin distributed fibre sensors. In: Jaroszewicz LR, editor. Proc. SPIE, Fifth Eur. Work. Opt. Fibre Sensors. Vol. 8794. Krakow, Poland; 2013. p. 87943J. DOI: 10.1117/12.2026296

[63] Dong Y, Bao X. High spatial resolution and long-distance BOTDA using differential Brillouin gain in a

dispersion shifted fiber. In: 20th Int. Conf. Opt. Fibre Sensors. Vol. 7503. 2009. p. 750384-4. DOI: 10.1117/12.848676

[64] Foaleng SM, Thévenaz L. Impact of Raman scattering and modulation instability on the performances of Brillouin sensors. Proceedings of SPIE The International Society for Optical Engineering. 2011;**7753**:77539V-775394V. DOI: 10.1117/12.885105

[65] Soto MA, Ricchiuti AL, Zhang L, Barrera D, Sales S, Thevenaz L. Time and frequency pump-probe multiplexing to enhance the signal response of Brillouin optical time-domain analyzers. Optics Express. 2014; **22**:28584-28595. DOI: 10.1364/OE.22.028584

[66] Voskoboinik A, Yilmaz OF, Willner AW, Tur M. Sweep-free distributed Brillouin time-domain analyzer (SF-BOTDA). Optics Express. 2011;**19**: B842-B847. DOI: 10.1364/OE.19.00B842

[67] Urricelqui J, Alem M, Sagues M, Thévenaz L, Loayssa A, Soto MA. Mitigation of modulation instability in Brillouin distributed fiber sensors by using orthogonal polarization pulses. In: Proc SPIE, 24th Int Conf Opt Fibre Sensors. Vol. 9634. 2015. p. 963433. DOI: 10.1117/12.2195292

[68] Minardo A, Bernini R, Zeni L, Thevenaz L, Briffod F. A reconstruction technique for long-range stimulated Brillouin scattering distributed fibre-optic sensors: Experimental results. Measurement Science and Technology. 2005;**16**:900-908. DOI: 10.1088/0957-0233/16/4/002

[69] Zornoza A, Minardo A, Bernini R, Loayssa A, Zeni L. Pulsing the probe wave to reduce nonlocal effects in brillouin optical time-domain analysis (BOTDA) sensors. IEEE Sensors Journal. 2011;**11**:1067-1068. DOI: 10.1109/JSEN.2010.2078805

[70] Dominguez-Lopez A, Angulo-Vinuesa X, Lopez-Gil A, Martin-Lopez S, Gonzalez-Herraez M. Non-local effects in dual-probe-sideband Brillouin optical time domain analysis. Optics Express. 2015;**23**:10341. DOI: 10.1364/OE.23.010341

[71] Iribas H, Urricelqui J, Mompó JJ, Mariñelarena J, Loayssa A. Non-local effects in Brillouin optical time-domain analysis sensors. Applied Sciences. 2017; **7**:761. DOI: 10.3390/app7080761

[72] Bernini R, Minardo A, Zeni L. Long-range distributed Brillouin fiber sensors by use of an unbalanced double sideband probe. Optics Express. 2011; **19**:23845. DOI: 10.1364/OE.19.023845

[73] Mompó JJ, Urricelqui J, Loayssa A. Brillouin optical time-domain analysis sensor with pump pulse amplification. Optics Express. 2015;**24**:1340-1348. DOI: 10.1364/OE.24.012672

[74] Urricelqui J, Sagues M, Loayssa A. Synthesis of Brillouin frequency shift profiles to compensate non-local effects and Brillouin induced noise in BOTDA sensors. Optics Express. 2014;**22**:18195. DOI: 10.1364/OE.22.018195

[75] Iribas H, Mariñelarena J, Feng C, Urricelqui J, Schneider T, Loayssa A. Effects of pump pulse extinction ratio in Brillouin optical time-domain analysis sensors. Optics Express. 2017;**25**: 27896-27911. DOI: 10.1364/OE.25.027896

[76] Feng C, Iribas H, Marinelaerña J, Schneider T, Loayssa A. Detrimental effects in Brillouin distributed sensors caused by EDFA transient. In: Conf. Lasers Electro-Optics; San Jose, Califonia, United States. 2017. p. JTu5A.85. DOI: 10.1364/CLEO_AT.2017.JTu5A.85

[77] Zornoza A, Olier D, Sagues M, Loayssa A. Brillouin distributed sensor using RF shaping of pump pulses.

Measurement Science and Technology. 2010;**21**:094021. DOI: 10.1088/0957-0233/21/9/094021

[78] Li W, Bao X, Li Y, Chen L. Differential pulse-width pair BOTDA for high spatial resolution sensing. Optics Express. 2008;**16**:21616. DOI: 10.1364/OE.16.021616

[79] Motil A, Danon O, Peled Y, Tur M. High spatial resolution BOTDA using simultaneously launched gain and loss pump pulses. In: Fifth Eur Work Opt Fibre Sensors. 2013. p. 87943L. DOI: 10.1117/12.2026670

[80] Kishida K, Li C. Pulse pre-pump-BOTDA technology for new generation of distributed strain measuring system. Structural Health Monitoring and Intelligent Infrastructure. 2005;**1**: 471-477

[81] Voskoboinik A, Wang J, Shamee B, Nuccio SR, Zhang L, Chitgarha M, et al. SBS-based Fiber optical sensing using frequency-domain simultaneous tone interrogation. Journal of Lightwave Technology. 2011;**29**:1729-1735. DOI: 10.1109/JLT.2011.2145411

[82] Bernini R, Minardo A, Zeni L. Dynamic strain measurement in optical fibers by stimulated Brillouin scattering. Optics Letters. 2009;**34**:2613-2615. DOI: 10.1364/OL.34.002613

[83] Jin C, Guo N, Feng Y, Wang L, Liang H, Li J, et al. Scanning-free BOTDA based on ultra-fine digital optical frequency comb. Optics Express. 2015;**23**:5277-5284. DOI: 10.1364/OE.23.005277